



RESEARCH LETTER

10.1002/2016GL068945

Key Points:

- Eddies in coastal upwelling systems contribute to export of coastal production
- Cyclonic and anticyclonic eddies have asymmetric roles in controlling biology
- Cyclonic eddies play a major role in redistributing and enhancing biology

Supporting Information:

- Supporting Information S1

Correspondence to:

F. Chenillat,
fchenillat@ucsd.edu

Citation:

Chenillat, F., P. J. S. Franks, and V. Combes (2016), Biogeochemical properties of eddies in the California Current System, *Geophys. Res. Lett.*, *43*, 5812–5820, doi:10.1002/2016GL068945.

Received 18 APR 2016

Accepted 27 MAY 2016

Accepted article online 31 MAY 2016

Published online 11 JUN 2016

Biogeochemical properties of eddies in the California Current System

Fanny Chenillat¹, Peter J. S. Franks¹, and Vincent Combes²

¹Integrative Oceanography Division, Scripps Institution of Oceanography, University of California San Diego, La Jolla, California, USA, ²College of Earth, Ocean, and Atmospheric Sciences, Oregon State University, Corvallis, Oregon, USA

Abstract The California Current System (CCS) has intense mesoscale activity that modulates and exports biological production from the coastal upwelling system. To characterize and quantify the ability of mesoscale eddies to affect the local and regional planktonic ecosystem of the CCS, we analyzed a 10 year-long physical-biological model simulation, using eddy detection and tracking to isolate the dynamics of cyclonic and anticyclonic eddies. As they propagate westward across the shelf, cyclonic eddies efficiently transport coastal planktonic organisms and maintain locally elevated production for up to 1 year (800 km offshore). Anticyclonic eddies, on the other hand, have a limited impact on local production over their ~6 month lifetime as they propagate 400 km offshore. At any given time ~8% of the model domain was covered by eddy cores. Though the eddies cover a small area, they explain ~50 and 20% of the transport of nitrate and plankton, respectively.

1. Introduction

The California Current System (CCS) is one of the four major Eastern Boundary Upwelling Systems (EBUS), characterized by upwelling of deep, nutrient-rich water at the coast, driving intense biological production and important fisheries. Like in other EBUS, eddies are omnipresent in the CCS [e.g., *Abbott and Zion*, 1985; *Kelly et al.*, 1998; *Strub and James*, 2000; *Stegmann and Schwing*, 2007; *Capet et al.*, 2008; *Chaigneau et al.*, 2009; *Kurian et al.*, 2011; *Chelton et al.*, 2011]. Forming near the coast, eddies have radii of 50–150 km, sea surface height anomalies of 5–10 cm, and propagate westward toward the open ocean with speeds of ~2 km d⁻¹. Being predominantly nonlinear features [*Chelton et al.*, 2011], eddies are able to trap coastal water, transporting it and the associated high biological biomass offshore from the coastal upwelling region [*Logerwell and Smith*, 2001; *Gruber et al.*, 2011; *Morales et al.*, 2012; *Combes et al.*, 2013; *Chenillat et al.*, 2015; *Nagai et al.*, 2015].

While the mesoscale eddy dynamics of the CCS have been well studied, the ecological roles of mesoscale activity in the CCS—and more widely in EBUS—are still unclear due to practical limitations (i.e., sparse field observations of individual eddies, observations from satellite being restricted to the sea surface, and significant computer resources needed for eddy-resolving coupled models). Some studies, mostly using models, have shown that eddies have a negative impact on coastal primary production by exporting coastal biomass and nutrients and subducting them below the euphotic layer while traveling offshore [*Gruber et al.*, 2011; *Nagai et al.*, 2015]. Other modeling and observational studies, on the other hand, have found that eddies are sites of locally enhanced biological activity [*Almazán-Becerril et al.*, 2012; *Stramma et al.*, 2013; *Mahadevan*, 2014; *Chenillat et al.*, 2015]. This apparent discrepancy emerges from the different perspectives used, with some studies examining the local impact of individual eddies, and others the net impact of mesoscale activity on biology integrated over a larger region. To clearly understand the ecological role of eddies in the CCS, a combination of these methods is required, giving a description of the properties of biogeochemical tracers averaged over multiple individual eddies. To date, there are limited studies describing average vertical distributions of temperature and salinity in eddies of the CCS [e.g., *Huyer et al.*, 1998; *Kurian et al.*, 2011; *Dong et al.*, 2012] or in EBUS, in general [see *Pegliasco et al.*, 2015, and references within]. Few recent studies have focused on the regional effects of mesoscale activity on the cross-shore export of phytoplankton-rich waters in the CCS [*Gruber et al.*, 2011; *Gaube et al.*, 2014; *Nagai et al.*, 2015], and none have simultaneously investigated the vertical structure of the ecosystem within eddies.

Here we compare spatially averaged fields to averages of individual eddies to quantify the overall effect of thousands of individual cyclonic and anticyclonic eddies in a 10 year numerical simulation of the CCS.

Compared to the recent studies [Gruber *et al.*, 2011; Nagai *et al.*, 2015], by creating eddy composites we not only evaluate the cross-shore export of coastal material, but we also investigate the spatial structure of the ecosystem within eddies and over the region. Our methods are described in section 2. In section 3, we explore the contrasting roles of cyclonic and anticyclonic eddies in the CCS in locally enhancing or decreasing biological concentrations and track those changes in depth distributions as the eddies propagate offshore. In the CCS, cyclonic eddies are important in (1) exporting biologically rich coastal water offshore and (2) maintaining high biological biomass that can only be explained by local vertical input within eddies. On average, anticyclones have a weak effect on biological activity, due to the high variability among ecosystems in anticyclonic eddies. A summary and concluding remarks are given in section 4.

2. Methods

2.1. Ocean Circulation Model

We investigate the biological effects of mesoscale dynamics in the CCS using the Regional Ocean Modeling System (ROMS), coupled to NEMURO (North Pacific Ecosystem Model for Understanding Regional Oceanography) [Kishi *et al.*, 2007], which is a complex ecosystem model (two types of nutrient, two phytoplankton classes, three zooplankton classes, and several detrital pools). ROMS is a three-dimensional, free-surface, hydrostatic, eddy-resolving primitive equation ocean model [Shchepetkin and McWilliams, 2005]. The physical model configuration (including surface forcings, boundary, and initial conditions) is the same as Capet *et al.* [2008], with a 5 km horizontal resolution covering the entire CCS (from the coast to ~1500 km offshore and from 24°N to 50°N). NEMURO has been tuned to reproduce the mean seasonal cycles of planktonic production in the CCS [Chenillat *et al.*, 2012, 2013].

The final state of a 30 year spin-up of the model (20 years for the physical model followed by 10 years for the coupled physical-biological model) was used as the initial condition of a 10 year run. Five-day averages of physical variables were archived and used to calculate the main eddy statistics in the CCS. This 5 km horizontal resolution model has been shown to realistically reproduce the mesoscale activity of the CCS when compared to altimetry observations [Capet *et al.*, 2008; Kurian *et al.*, 2011] including permanent eddies generated from the CCS [Strub and James, 2000], and coastal eddies formed through baroclinic instabilities in the CCS [Capet and Carton, 2004].

This coupled model showed good agreement with observations from the California Cooperative Oceanic Fisheries Investigations (CalCOFI) program [Chenillat *et al.*, 2015, their Figure 3]; in particular, the Chl *a* maximum is dominated by large phytoplankton (diatom-like, requiring silicon) close to shore, and by small phytoplankton (nondiatom-like, not requiring silicon) offshore; the planktonic assemblage in a cyclonic eddy was dominated by small-size classes in the surface mixed layer and by large-size classes below the mixed layer.

2.2. Reynolds Decomposition

We quantified the eddy contribution to the advective flux divergence of the tracer budgets by performing a Reynolds decomposition. The total cross-shore advection terms were decomposed into the mean and the eddy contribution [Capet *et al.*, 2008]:

$$\overline{u \cdot c} = \overline{u} \cdot \overline{c} + \overline{u' \cdot c'}$$

with *c* the tracer concentration and *u* the cross shore (i.e., normal to the general orientation of the coastline) velocity field. Primed quantities are deviations from the 10 year averaged monthly mean climatology, which is represented by overbars.

2.3. Eddy Detection Method

To quantify average mesoscale eddy properties, we detected eddies in the 10 year run using the Okubo-Weiss method [Okubo, 1970; Weiss, 1991; Isern-Fontanet *et al.*, 2003; Chelton *et al.*, 2007; Kurian *et al.*, 2011], which is based on the computation of the Okubo-Weiss parameter (*W*):

$$W = S_n^2 + S_s^2 - \zeta^2$$

where *S_n* and *S_s* are the normal and shear components of the strain and ζ is the relative vorticity of the flow. These quantities are defined by

$$S_n = \frac{\partial u}{\partial x} - \frac{\partial v}{\partial y}, \quad S_s = \frac{\partial v}{\partial x} + \frac{\partial u}{\partial y}, \quad \zeta = \frac{\partial v}{\partial x} - \frac{\partial u}{\partial y},$$

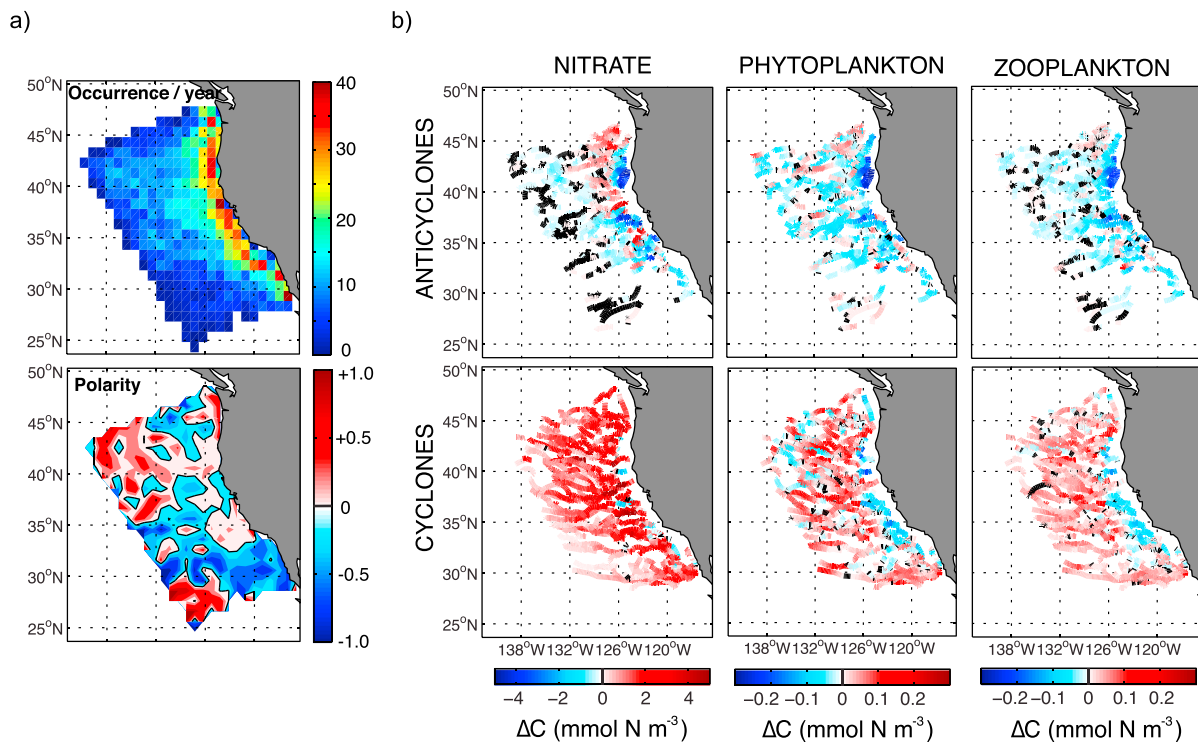


Figure 1. (a) (top) Average number of surface eddies per year in $1^\circ \times 1^\circ$ boxes, computed over the 10 year model run, and (bottom) eddy polarity $((N_a - N_c)/(N_a + N_c))$, with N_a and N_c the number of anticyclones (red) and cyclones (blue), respectively. A positive (negative) polarity represents dominance of anticyclones (cyclones). (b) Tracks of long-lived anticyclonic (top) and cyclonic eddies (bottom), with superimposed euphotic-zone-average anomalies of nitrate (left), phytoplankton biomass (middle), and zooplankton biomass (right) within eddies compared to the local annual climatological mean. The black portions of some tracks denote a null anomaly.

respectively, where u and v are the eastward and the northward velocities. A vorticity-dominant field, in which the rotation of the flow dominates over its deformation, indicates the potential location of eddies; this corresponds to negative values of W . We chose a threshold value of $-5 \times 10^{-11} \text{ s}^{-2}$ to identify eddy cores [Chelton *et al.*, 2007], i.e., the part of the eddy that presumably is in solid body rotation [e.g., Oh and Zhurbas, 2000; Lilly and Rhines, 2002; Yelland and Crawford, 2005; Chelton *et al.*, 2011]. To remove non-eddy structures from the closed contour analysis, we required that an eddy must fit a circular shape with an error less than 40% (see details in Kurian *et al.* [2011]) and with a minimum radius of 15 km. The radius, position, and polarity (cyclonic or anticyclonic) of eddies passing these criteria were saved. We saved eddies with a surface circulation signature, including near-surface eddies whose dominant signature was subsurface, but still had a surface signature. We neglected eddies occurring below the surface and without a surface signature [Kurian *et al.*, 2011; Hormazabal *et al.*, 2013]; such eddies have only weak effects on the biogeochemical tracers.

2.4. Eddy Tracking

Eddies were tracked automatically in the 5 day average outputs by comparing eddy center positions and radii at consecutive time steps over the entire run. To avoid the tracking method switching among eddies, an eddy must travel less than one eddy diameter between successive 5 day time steps. Only long-lived (>90 days) eddies were tracked to provide a clear synthetic view of the lateral eddy transport. Some eddy trajectories had a gap in time when the eddies could not pass the identification criteria due to strong deformation events. Though trajectories that last less than 90 days were not included, our analyses are not sensitive to these restrictions.

From the eddy trajectories we calculate the speed, the direction of propagation, and the biogeochemical properties as they evolve along the eddy paths.

2.5. Average Eddy Analysis

To quantify the vertical and radial structure of properties in the eddies, we performed an average eddy analysis—or composite analysis—on all the detected eddies. The computed eddy radius R corresponds to the radius of the eddy core. To include both the eddy core and the area surrounding the eddy, we extracted

the eddy properties over a cross-shore transect centered on the eddy from $-3R$ to $+3R$. The horizontal coordinates were then normalized by the radius R of each eddy, and physical and biogeochemical variables were averaged over all the eddies in this normalized coordinate system (eddy center at 0 and edge of the eddy core at ± 1). These horizontally normalized distributions included temperature, salinity, nitrate concentrations, and total phytoplankton and zooplankton biomasses.

Along with the cross-shore average of properties across eddies, we also calculated a zonal average of all eddy cores (from $-1R$ to $+1R$), for each property. This diagnostic was performed using all individual eddies. The distance of each eddy from the coast is known, allowing us to create cross-shore sections of (separately) cyclonic eddies and anticyclonic eddies, these sections being averaged north-to-south along the coast. These are the cross-shore cyclonic and anticyclonic eddy sections and contain only eddy properties. They were compared to an annual climatological cross-shore section (averaged over 10 years) by computing the anomalies of the eddy sections relative to the annual climatological section.

Individual eddy property anomalies were calculated relative to the annual climatological mean at each grid point over the 10 year run ($\overline{C}_{10 \text{ years}}$). The annual climatological mean was subtracted from the local eddy-core euphotic-zone averages (C_{eddy}) to obtain the local anomaly:

$$\Delta C = \int_0^{z_{\text{euphotic}}} C_{\text{eddy}}(x, y, z) dz - \int_0^{z_{\text{euphotic}}} \overline{C}_{10 \text{ years}}(x, y, z) dz$$

3. Results and Discussion

Our eddy statistics in the CCS were similar to previous investigations (Figure 1) [e.g., *Stegmann and Schwing, 2007; Chaigneau et al., 2009; Kurian et al., 2011*]. Over our 10 year model run, archived every 5 days, we identified a total of 16,808 cyclones and 16,553 anticyclones, i.e., an average of 168 cyclones and 166 anticyclones per year. About 40% of the eddies were found within 200 km of the coast, which represents only 20% of the model domain; the frequency of eddy occurrence decreased with distance offshore (Figure 1). This is consistent with observations of CCS eddies that are generated near the coast and move westward [*Pares-Sierra et al., 1993; Kelly et al., 1998; Strub and James, 2000; Stegmann and Schwing, 2007; Kurian et al., 2011*]. Within 200 km off the coast, cyclonic eddies were more abundant in the fall; there was no seasonal trend for anticyclonic eddies. Higher mesoscale activity during the fall was observed in CCS altimetry data [*Strub and James, 2000*], but is inconsistent with some analyses that found a peak in the winter [*Stegmann and Schwing, 2007*] or no clear seasonal cycle [*Kurian et al., 2011*]. Differences observed with *Kurian et al. [2011]*, who used the same model, result from the eddy-identification criteria. We used all detected individual eddies (see section 2.4), while *Kurian et al. [2011]* used only eddies that could be tracked for at least 30 days. There was no pronounced north-south trend in eddy occurrence [*Nagai et al., 2015*]. Near the coast there is more anticyclonic eddies north of Point Conception ($\sim 34^\circ\text{N}$) and cyclonic eddies to the south [e.g., *Stegmann and Schwing, 2007; Kurian et al., 2011; Chaigneau et al., 2009*, their Figure 2b].

The average size of the cores of cyclonic eddies was ~ 25 km, and ~ 20 km for anticyclonic eddies, again similar to *Kurian et al. [2011]*. Cyclonic and anticyclonic eddies had a SSH anomaly of 6 and 4 cm at $3R$ (i.e., at the edge of an average eddy), respectively, the same order of magnitude as found in satellite data [*Gaube et al., 2014*]. At any given time, about 4.6% of the area of the model domain was covered by cyclonic eddy cores and 3.5% by anticyclonic eddy cores. Using Reynolds decomposition, we estimate that despite their relatively small area, eddies accounted for 50, 18, and 24% of the offshore export of nitrate, total phytoplankton, and total zooplankton from the 200 km coastal band, the remainder (50, 82, and 76%) being exported by the mean Ekman transport.

We tracked 158 cyclonic and 121 anticyclonic long-lived eddies (>90 days), all of which tended to propagate toward the west; cyclonic eddies propagated $\sim 5^\circ$ northwest, while anticyclonic eddies propagated 15° southwest, similar to results from *Kurian et al. [2011]*. This deflection is due to the beta effect [e.g., *McWilliams and Flierl, 1979; Cushman-Roisin, 1994*]. The average lifetimes of tracked cyclonic and anticyclonic eddies were 170 and 150 days, respectively, though some persisted for more than 1 year. Our stringent eddy criteria often caused the tracking algorithm to lose an eddy part-way through its life, and then pick it up again later, giving shorter overall eddy durations than tracking eddies by eye. The eddies propagated across shore at an average speed

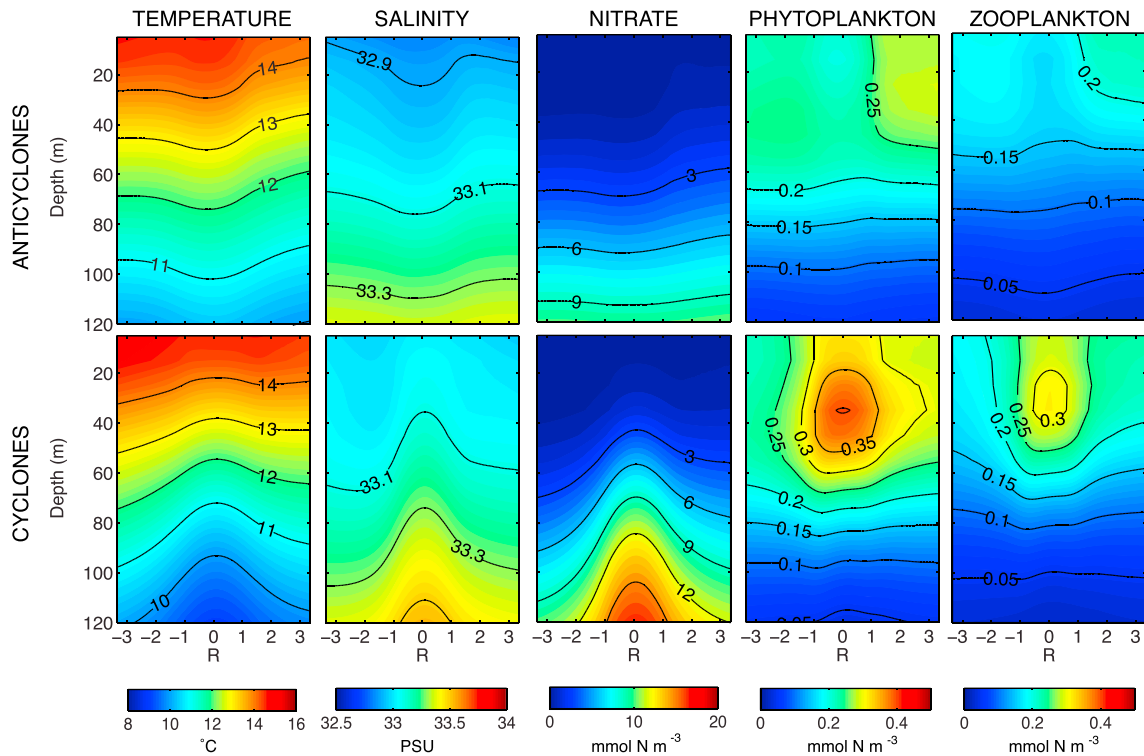


Figure 2. Average properties of (top row) anticyclonic and (bottom row) cyclonic eddies. From left to right: temperature, salinity, nitrate, phytoplankton biomass, and zooplankton biomass. The composites represent the average profiles across eddies, with the eddy core centered at 0, and R the radius of the eddy core (positive R represents the coastal side).

of $\sim 2 \text{ km d}^{-1}$ [Stegmann and Schwing, 2007; Chelton et al., 2011; Kurian et al., 2011] and would take more than a year to cross the 1500 km model domain. For a more complete description of the eddy dynamics from this model, see Kurian et al. [2011].

The cross-shore average properties of cyclonic and anticyclonic eddies were quite distinct (Figure 2): cyclonic eddies showed a signature down to 600 m (not shown) with an upward doming of up to 50 m of isotherms, isohalines, and isolines of nitrate. Anticyclonic eddies had a deeper signature (down to 800 m, not shown) and relatively weak ($<10 \text{ m}$) depressions of these properties in the eddy core [Kurian et al., 2011]. This asymmetric response may be due to the inclusion of near-surface eddies in the averaging.

The upward doming of nitrate in the core of cyclonic eddies was associated with a local doubling (relative to the waters surrounding the eddies) of the biomass of the subsurface maxima of phytoplankton and zooplankton, similar to individual eddy observations in EBUS [e.g., Correa-Ramirez et al., 2007; Almazán-Becerril et al., 2012]. The weak hydrographic signature of anticyclonic eddies was associated with a similarly weak biological signature, with slight deficits in phytoplankton and zooplankton biomass in the eddy core, near the surface ($\sim 15 \text{ m}$). Variability was greater in anticyclonic eddies, leading to a smaller average anomaly signature (Figure 2). The subsurface biomass maxima were centered at $\sim 35 \text{ m}$ depth in cyclonic eddies, about half the 83 m euphotic depth.

We found no significant latitudinal differences in the euphotic-zone-average biological properties of eddy cores, although the temperature and salinity tended to decrease with increasing latitude. Eddies formed at the central coast had slightly (but not significantly) more nitrate and plankton biomass in their cores (not shown). Differences in biological properties between cyclonic and anticyclonic eddies were more pronounced at lower latitudes (not shown).

The euphotic-zone-average biological properties of cyclonic and anticyclonic eddy cores showed no significant seasonal differences (see the supporting information). Biogeochemical tracer concentrations tended to be higher in cyclonic eddies than in anticyclonic eddies, although this difference was not significant. For both eddy polarities, there was a general seasonal trend in biogeochemical concentrations that matched the

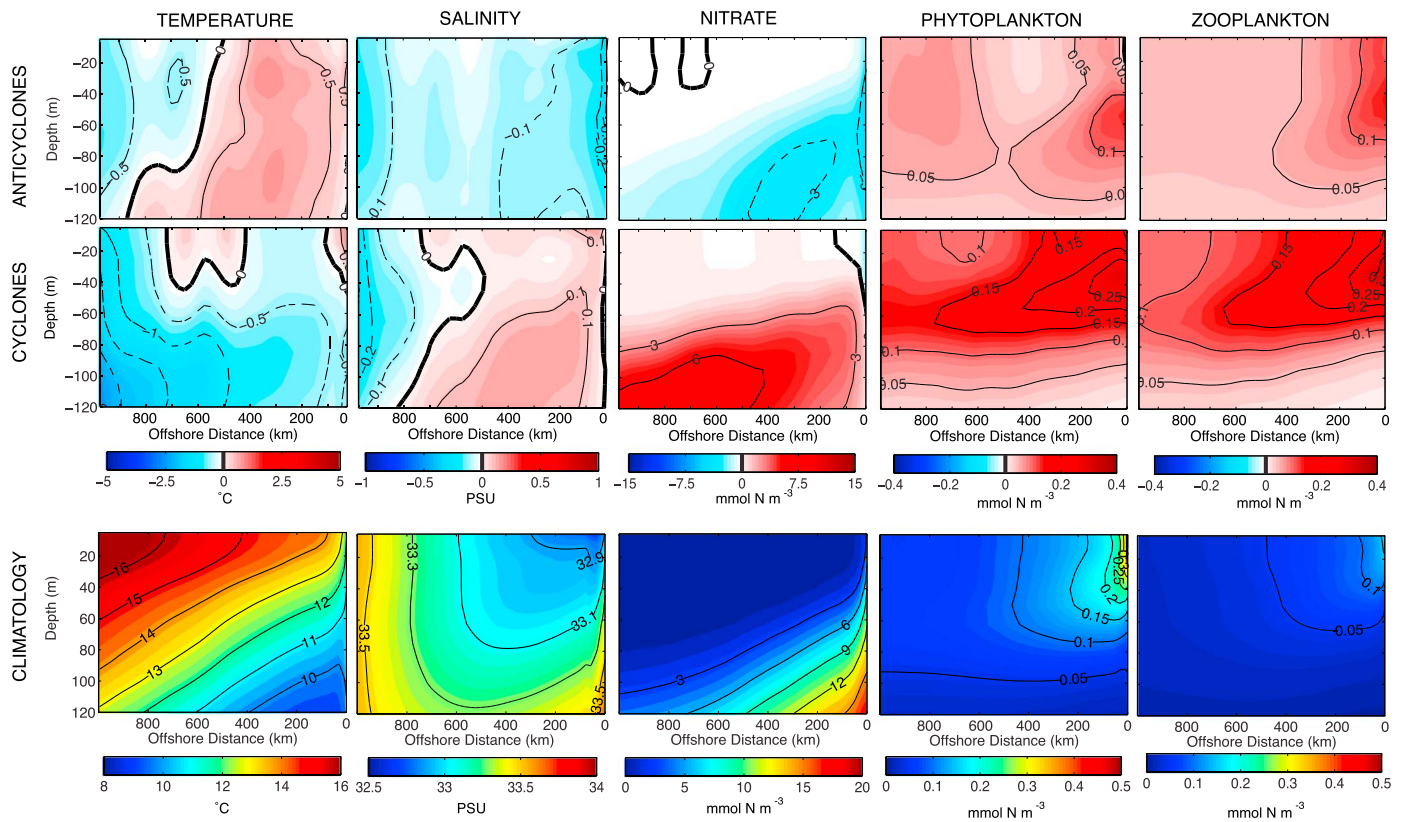


Figure 3. Cross-shore vertical sections of anomalies of properties in (top row) anticyclonic eddy cores and (middle row) cyclonic eddy cores compared to cross-shore vertical sections of (bottom row) climatological north-south-averages of (left to right) temperature, salinity, nitrate, phytoplankton biomass, and zooplankton biomass.

biological seasonal variations of coastal upwelling systems (the eddy source waters), with a peak of nitrate concentrations and plankton biomass in spring-summer (not shown) [see *Chenillat et al.*, 2012, 2013].

Hydrographically, anticyclonic eddies were only slightly different from the climatological mean, while cyclonic eddies were noticeably colder and saltier at depth (Figure 3). In all cases the isolines of temperature and salinity deepened with distance offshore, although this deepening was weaker in cyclonic eddies, which maintained cooler temperatures at shallower depths offshore than the mean. This deepening of isopycnals across shore is consistent with previous studies [Barth *et al.*, 2002; Bograd and Mantyla, 2005; Pegliasco *et al.*, 2015] and observations from the CalCOFI program (see Figure 5 of *Chenillat et al.* [2013]).

The anomalies of concentrations of nitrate, phytoplankton, and zooplankton (Figures 1 and 3) highlight the spatial variability induced by eddies. As expected from our previous results, cyclonic eddies contained more nitrate than the local average ($+4 \text{ mmol N m}^{-3}$) when located close to the shore; as the eddies propagated offshore, this difference slowly decreased. Cyclonic eddies had a clear positive anomaly of both phytoplankton ($+0.2 \text{ mmol N m}^{-3}$) and zooplankton ($+0.1 \text{ mmol N m}^{-3}$) over the lifetime of the eddy, although these anomalies were sometimes negative near the coast ($-0.1 \text{ mmol N m}^{-3}$). These anomalously high coastal nitrate concentrations were carried with the cyclonic eddies, fueling the ecosystem as they propagated across shore [Chenillat *et al.*, 2015]. Anticyclonic eddies, on the other hand, showed mixtures of positive and negative nitrate anomalies (from -2 to 2 mmol N m^{-3}) and biological anomalies (from -0.1 to $0.05 \text{ mmol N m}^{-3}$), both of which were weaker on average than those found in cyclonic eddies. Anticyclonic eddies contained less euphotic zone nitrate than the local average. The anomalies developed close to shore soon after the anticyclonic eddies were formed and tended to decay as the eddies moved offshore.

Cyclonic eddy cores had significantly enhanced biomass of all planktonic groups compared to anticyclonic eddy cores. However, on average the relative proportions of different planktonic groups were the same in both types of eddies: 45% and 55% of small and large phytoplankton, respectively, and 20%, 35%, and

45% of small, large, and predator zooplankton, respectively. Similar proportions were diagnosed in the mature stage of a cyclonic eddy from a numerical simulation of the southern CCS [Chenillat *et al.*, 2015].

Chenillat *et al.* [2015] showed that the enhanced productivity and biomass in a cyclonic eddy was a consequence of the upward doming of the nitracline into the euphotic zone, combined with Ekman pumping of nitrate into the euphotic zone, i.e., a local upwelling driven by the surface wind stress curl. Although the Ekman pumping was not particularly high in the eddies relative to the surrounding waters, the shallow nitracline in the eddy core allowed an increased upward nitrate flux there. This enhanced nitrate flux drove increased biomasses of both small and large phytoplankton and zooplankton in the waters between the base of the mixed layer and the bottom of the euphotic zone. The analyses presented here show that the dynamics revealed in the detailed examination of a single cyclonic eddy [Chenillat *et al.*, 2015] can be generalized to all cyclonic eddies in the CCS. The average cyclonic eddy is formed within 200 km of the coast and propagates offshore toward the northwest. It carries with it enhanced biomasses of phytoplankton and zooplankton; although these biomasses decay with time and distance offshore, cyclonic eddies remain significantly enhanced compared to the local mean, or to anticyclonic eddies, over their lifetime.

The persistent local enhancement of biological properties in cyclonic eddies suggests that the influence of the core waters present at eddy formation continues through the life of the eddy. One conclusion is that the eddies likely have relatively little exchange with their surrounding waters [e.g., Sangrà *et al.*, 2005; Chenillat *et al.*, 2015]: because eddies are nonlinear features [Chelton *et al.*, 2011], the eddy properties remain distinct compared to surrounding waters. The regions of significant biological enhancement in cyclonic eddies were persistently subsurface—well below the depths visible to satellite remote sensing. Thus, the biological signatures of cyclonic eddies in particular may be consistently underestimated by satellite analyses of eddy properties.

Through eddy tracking it appears that cyclonic eddies play a fundamental role in the cross-shore export of coastal waters and biota [e.g., Logerwell *et al.*, 2001; Stegmann and Schwing, 2007; Gruber *et al.*, 2011; Nagai *et al.*, 2015]. Furthermore, the sustained enhancement of phytoplankton and zooplankton in these eddies—even with losses due to sinking and horizontal mixing—suggests that local physical inputs of nitrate are an important driver of the biological dynamics during the eddy lifetime [e.g., Chenillat *et al.*, 2015].

In contrast to cyclonic eddies, anticyclonic eddies appear to have a limited impact on the planktonic ecosystem [Nagai *et al.*, 2015]. Slight deficits in phytoplankton and zooplankton biomass propagate across shore with the anticyclonic eddies, although these are weak relative to the local mean. This is in contrast to some observations of a positive impact of anticyclonic eddies localized close to shore (Figures 1 and 3). However, when averaged over the entire model domain, the anticyclonic signal is weak (Figure 2).

Our findings are consistent with field and satellite studies of individual eddies showing that both cyclonic and anticyclonic eddies can trap coastal water and enhance local production nearshore [e.g., Correa-Ramirez *et al.*, 2007; Almazán-Becerril *et al.*, 2012; Stramma *et al.*, 2013; Gaube *et al.*, 2014]. However, in anticyclonic eddies such intensification of biological production is not uniform, being weaker and evolving less dramatically than in cyclonic eddies [Nagai *et al.*, 2015; Gaube *et al.*, 2014]. This local intensification of biological production in cyclones is associated with coastal upwelling during the early stages of the formation of the eddy. Thus, cyclonic eddies represent a key component of the spatial transport of biogeochemical tracers and of the local intensification of biological activity far offshore. This finding complements Gruber *et al.* [2011] and Nagai *et al.* [2015], who suggested that eddies drive a loss of coastal material through subduction below the euphotic layer. Our investigation showed that cyclonic eddies, in particular, efficiently transport coastal material hundreds of kilometers offshore, maintaining elevated biological properties for up to one year (800 km offshore) and forming an efficient cross-shelf transport pathway, confirming recent findings [Nagai *et al.*, 2015]. However, compared to these recent studies [Gruber *et al.*, 2011; Nagai *et al.*, 2015], our study offers new insights into the average vertical structure of the ecosystem within eddies, describing the prominent role of cyclonic eddies in maintaining a relatively constant ecosystem structure and persistently elevated biomass during its transit from the coast to the open ocean.

4. Summary and Conclusions

Biogeochemical properties in eddies of the CCS were studied using a coupled physical-biological model with a 5 km horizontal resolution model. This model accurately reproduced both the eddy mesoscale activity generated at the coast and the main biological properties of the CCS.

Applying an eddy-detection and eddy-tracking algorithm to the 10 year long run allowed us to quantify biogeochemical tracers within individual cyclonic and anticyclonic eddies. Averaging >16,000 cyclonic eddies, we found a strong positive biological signature associated with the doming of isolines within the core. This was in contrast to the average of >16,000 anticyclonic eddies, which showed a weak signature due to the mixture of dynamics associated with such eddies.

While propagating offshore, cyclonic eddies are more efficient than anticyclonic in trapping and redistributing biogeochemical material from coastal source waters. However, both eddy polarities transport material farther offshore than the long-term average total transport (which includes Ekman transport). This intense eddy activity explains ~50 and 20% of the transport of nitrate and plankton, respectively, although the cyclonic eddies cover only about 4% of the domain.

We found no clear/significant latitudinal or seasonal gradient in the frequency of occurrence or hydrographic/biological properties of the eddies.

Because of their inherent structure, cyclonic eddies play a fundamental role in modulating the biogeochemistry and ecosystem of upwelling systems. Indeed, the ecosystem within cyclonic eddies benefits from both the coastal upwelling source waters (at regional scales) and from local vertical fluxes within the eddy. Nearshore, these complementary processes initialize cyclonic eddies with more than the regional average of biogeochemical tracers. Cyclonic eddies are thus important features of coastal upwelling systems by (1) efficiently redistributing material from the coastal upwelling region by trapping and transporting water and (2) fueling local production while traveling offshore, through the combination of local upwelling and Ekman pumping. Contrastingly, anticyclonic eddies play a weak role in the biogeochemistry and ecosystems of upwelling systems: although they can trap water, they are less efficient in transporting water offshore due to their dynamics.

Acknowledgments

This work was supported by CCE-LTER program (NSF Grant, DEB#0832652). The altimeter products were produced by Ssalto/Duacs and distributed by Aviso, with support from CNES (<http://www.aviso.oceanobs.com/duac>). The boundaries and surface forcing used for the model are available from Comprehensive Ocean-Atmosphere Data Set (<http://iridl.ldeo.columbia.edu/SOURCES/COADS/>), Advanced Very High Resolution Radiometer (<http://noaa.gov/NOAASIS/ml/avhrr.html>), Quick Scatterometer - QuikScat (<http://www.remss.com/missions/qscat>), and Ocean General Circulation Model for the Earth Simulator (<http://www.jamstec.go.jp/esc/research/AtmOcn/product/ofes.html>). All the numerical runs were performed with the Caparmor high-performance computer facilities—Ifremer. The numerical data set and algorithms that support this article are available upon request to the authors.

References

- Abbott, M. R., and P. M. Zions (1985), Satellite observations of phytoplankton variability during an upwelling event, *Cont. Shelf Res.*, *4*(6), 661–680, doi:10.1016/0278-4343(85)90035-4.
- Almazán-Becerril, A., D. Rivas, and E. García-Mendoza (2012), The influence of mesoscale physical structures in the phytoplankton taxonomic composition of the subsurface chlorophyll maximum off western Baja California, *Deep Sea Res. Part I*, *70*, 91–102, doi:10.1016/j.dsr.2012.10.002.
- Barth, J. A., T. J. Cowles, P. M. Kosro, R. K. Shearman, A. Huyer, and R. L. Smith (2002), Injection of carbon from the shelf to offshore beneath the euphotic zone in the California Current, *J. Geophys. Res.*, *107*(C6), 3057, doi:10.1029/2001JC000956.
- Bograd, S. J., and A. W. Mantyla (2005), On the subduction of upwelled waters in the California Current, *J. Mar. Res.*, *63*, 863–885.
- Capet, X. J., and X. J. Carton (2004), Nonlinear regimes of baroclinic boundary currents, *J. Phys. Oceanogr.*, *34*, 1400–1409, doi:10.1175/1520-0485(2004)034<1400:NROBBC>2.0.CO;2.
- Capet, X., F. Colas, J. C. Mc Williams, P. Penven, and P. Marchesiello (2008), Eddies in eastern boundary subtropical upwelling systems, *Geophys. Monogr.*, 1–18.
- Chaigneau, A., G. Eldin, and B. Dewitte (2009), Eddy activity in the four major upwelling systems from satellite altimetry (1992–2007), *Prog. Oceanogr.*, *83*(1–4), 117–123, doi:10.1016/j.pocean.2009.07.012.
- Chelton, D. B., M. G. Schlax, R. M. Samelson, and R. A. de Szoeke (2007), Global observations of large oceanic eddies, *Geophys. Res. Lett.*, *34*, L15606, doi:10.1029/2007GL030812.
- Chelton, D. B., M. G. Schlax, and R. M. Samelson (2011), Global observations of nonlinear mesoscale eddies, *Prog. Oceanogr.*, *91*(2), 167–216, doi:10.1016/j.pocean.2011.01.002.
- Chenillat, F., P. Rivière, X. Capet, E. Di Lorenzo, and B. Blanke (2012), North Pacific Gyre Oscillation modulates seasonal timing and ecosystem functioning in the California Current upwelling system, *Geophys. Res. Lett.*, *39*, L01606, doi:10.1029/2011GL049966.
- Chenillat, F., P. Rivière, X. Capet, P. J. S. Franks, and B. Blanke (2013), California coastal upwelling onset variability: Cross-shore and bottom-up propagation in the planktonic ecosystem, *PLoS One*, *8*(5), e62281, doi:10.1371/journal.pone.0062281.
- Chenillat, F., P. J. S. Franks, P. Rivière, X. Capet, N. Grima, and B. Blanke (2015), Plankton dynamics in a cyclonic eddy in the Southern California Current System, *J. Geophys. Res. Oceans*, *120*, 5566–5588, doi:10.1002/2015JC010826.
- Combes, V., F. Chenillat, E. Di Lorenzo, P. Rivière, M. D. Ohman, and S. J. Bograd (2013), Cross-shore transport variability in the California Current: Ekman upwelling vs. eddy dynamics, *Prog. Oceanogr.*, *109*, 78–89, doi:10.1016/j.pocean.2012.10.001.
- Correa-Ramirez, M. A., S. Hormazabal, and G. Yuras (2007), Mesoscale eddies and high chlorophyll concentrations off central Chile (29°–39°S), *Geophys. Res. Lett.*, *34*, L12604, doi:10.1029/2007GL029541.
- Cushman-Roisin, B. (1994), *Introduction to Geophysical Fluid Dynamics*, 320 pp., Prentice Hall, N. J.
- Dong, C., X. Lin, Y. Liu, F. Nencioli, Y. Chao, Y. Guan, D. Chen, T. Dickey, and J. C. McWilliams (2012), Three-dimensional oceanic eddy analysis in the Southern California Bight from a numerical product, *J. Geophys. Res.*, *117*, C00H14, doi:10.1029/2011JC007354.
- Gaube, P., D. J. McGillicuddy Jr., D. B. Chelton, M. J. Behrenfeld, and P. G. Strutton (2014), Regional variations in the influence of mesoscale eddies on near-surface chlorophyll, *J. Geophys. Res. Oceans*, *119*, 8195–8220, doi:10.1002/2014JC010111.
- Gruber, N., Z. Lachkar, H. Frenzel, P. Marchesiello, M. Münnich, J. C. McWilliams, T. Nagai, and G.-K. Plattner (2011), Eddy-induced reduction of biological production in eastern boundary upwelling systems, *Nat. Geosci.*, *4*(11), 787–792, doi:10.1038/ngeo1273.
- Hormazabal, S., V. Combes, C. E. Morales, M. A. Correa-Ramirez, E. Di Lorenzo, and S. Nuñez (2013), Intrathermocline eddies in the coastal transition zone off central Chile (31–41°S), *J. Geophys. Res. Oceans*, *118*, 4811–4821, doi:10.1002/jgrc.20337.
- Huyer, A., J. A. Barth, P. M. Kosro, R. K. Shearman, and R. L. Smith (1998), Upper-ocean water mass characteristics of the California Current, summer 1993, *Deep Sea Res. Part II*, *45*, 1411–1442.
- Isern-Fontanet, J., E. García-Ladona, and J. Font (2003), Identification marine eddies from altimetric maps, *J. Atmos. Oceanic Technol.*, *20*(5), 772–778, doi:10.1175/1520-0426(2003)20<772:IOEFA>2.0.CO;2.

- Kelly, K. A., R. C. Beardsley, R. Limeburner, K. H. Brink, J. D. Paduan, and T. K. Chereskin (1998), Variability of the near-surface eddy kinetic energy in the California Current based on altimetric, drifter, and moored current data, *J. Geophys. Res.*, *103*(C6), 13,067–13,083, doi:10.1029/97JC03760.
- Kishi, M. J., et al. (2007), NEMURO—A lower trophic level model for the North Pacific marine ecosystem, *Ecol. Modell.*, *202*(1-2), 12–25, doi:10.1016/j.ecolmodel.2006.08.021.
- Kurian, J., F. Colas, X. Capet, J. C. McWilliams, and D. B. Chelton (2011), Eddy properties in the California Current System, *J. Geophys. Res.*, *116*, C08027, doi:10.1029/2010JC006895.
- Lilly, J. M., and P. B. Rhines (2002), Coherent eddies in the Labrador Sea observed from a mooring, *J. Phys. Oceanogr.*, *32*, 585–598, doi:10.1175/1520-0485.
- Logerwell, E. A., and P. E. Smith (2001), Mesoscale eddies and survival of late stage Pacific sardine (*Sardinops sagax*) larvae, *Fish. Oceanogr.*, *10*(1), 13–25, doi:10.1046/j.1365-2419.2001.00152.x.
- Logerwell, E. A., B. Lavaniegos, and P. E. Smith (2001), Spatially-explicit bioenergetics of Pacific sardine in the Southern California Bight: Are mesoscale eddies areas of exceptional prerecruit production?, *Prog. Oceanogr.*, *49*(1-4), 391–406, doi:10.1016/S0079-6611(01)00032-5.
- Mahadevan, A. (2014), Eddy effects on biogeochemistry, *Nature*, *506*, 168–169, doi:10.1038/nature13048.
- McWilliams, J. C., and G. R. Flierl (1979), On the evolution of isolated, nonlinear vortices (numerical models of ocean circulation), *J. Phys. Oceanogr.*, doi:10.1175/1520-0485(1979)009<1155:OTEIOIN>2.0.CO;2.
- Morales, C. E., S. Hormazabal, M. Correa-Ramirez, O. Pizarro, N. Silva, C. Fernandez, V. Anabalón, and M. L. Torreblanca (2012), Mesoscale variability and nutrient–phytoplankton distributions off central-southern Chile during the upwelling season: The influence of mesoscale eddies, *Prog. Oceanogr.*, *104*, 17–29, doi:10.1016/j.pocean.2012.04.015.
- Nagai, T., N. Gruber, H. Frenzel, Z. Lachkar, J. C. McWilliams, and G.-K. Plattner (2015), Dominant role of eddies and filaments in the offshore transport of carbon and nutrients in the California Current System, *J. Geophys. Res. Oceans*, *120*, 5318–5341, doi:10.1002/2015JC010889.
- Oh, I. S., and V. Zhurbas (2000), Study of spatial spectra of horizontal turbulence in the ocean using drifter data, *J. Phys. Oceanogr.*, *30*(7), 1790–1801, doi:10.1175/1520-0485(2000)030<1790:SOSSOH>2.0.CO;2.
- Okubo, A. (1970), Horizontal dispersion of floatable particles in the vicinity of velocity singularities such as convergences, *Deep Sea Res. Oceanogr. Abstr.*, *17*(3), 445–454, doi:10.1016/0011-7471(70)90059-8.
- Pares-Sierra, A., W. B. White, and C.-K. Tai (1993), Wind-driven coastal generation of annual mesoscale eddy activity in the California Current, *Am. Meteorol. Soc.*, *23*(66), 1110–1121, doi:10.1175/1520-0485(1993).
- Pegliasco, C., A. Chaigneau, and R. Morrow (2015), Main eddy vertical structures observed in the four major Eastern Boundary Upwelling Systems, *J. Geophys. Res. Oceans*, *120*, 6008–6033, doi:10.1002/2015JC010950.
- Sangrà, P., J. L. Pelegrí, A. Hernández-Guerra, I. Arregui, J. M. Martín, A. Marrero-Díaz, A. Martínez, A. W. Ratsimandresy, and A. Rodríguez-Santana (2005), Life history of an anticyclonic eddy, *J. Geophys. Res.*, *110*, C03021, doi:10.1029/2004JC002526.
- Shchepetkin, A. F., and J. C. McWilliams (2005), The regional oceanic modeling system (ROMS): A split-explicit, free-surface, topography-following-coordinate oceanic model, *Ocean Modell.*, *9*(4), 347–404, doi:10.1016/j.ocemod.2004.08.002.
- Stegmann, P. M., and F. Schwing (2007), Demographics of mesoscale eddies in the California Current, *Geophys. Res. Lett.*, *34*, L14602, doi:10.1029/2007GL029504.
- Stramma, L., H. W. Bange, R. Czeschel, A. Lorenzo, and M. Frank (2013), On the role of mesoscale eddies for the biological productivity and biogeochemistry in the eastern tropical Pacific Ocean off Peru, *Biogeosciences*, *10*, 7293–7306, doi:10.5194/bg-10-7293-2013.
- Strub, P. T., and C. James (2000), Altimeter-derived variability of surface velocities in the California Current System: 2. Seasonal circulation and eddy statistics, *Deep-Sea Res. Part II*, *47*(5-6), 831–870, doi:10.1016/S0967-0645(99)00129-0.
- Weiss, J. (1991), The dynamics of enstrophy transfer in two-dimensional hydrodynamics, *Phys. D*, *48*(2-3), 273–294, doi:10.1016/0167-2789(91)90088-Q.
- Yelland, D., and W. R. Crawford (2005), Currents in Haida Eddies, *Deep-Sea Res. Part II*, *52*(7-8), 875–892, doi:10.1016/j.dsr2.2005.02.010.